POLITECNICO MILANO 1863

RE.PUBLIC@POLIMI
Research Publications at Politecnico di Milano

Permanent link to this version
http://hdl.handle.net/11311/1062970

PAPER • OPEN ACCESS

A POD reduced-order model for wake steering control

To cite this article: A Fortes-Plaza *et al* 2018 *J. Phys.: Conf. Ser.* **1037** 032014

View the article online for updates and enhancements.

IOP ebooks™

Bringing you innovative digital publishing with leading voices to create your essential collection of books in STEM research.

Start exploring the collection - download the first chapter of every title for free.

A POD reduced-order model for wake steering control

A Fortes-Plaza[1]**, F Campagnolo**[1]**, J Wang**[1]**, C Wang**[1] **and CL Bottasso**[1,2]

[1] Wind Energy Institute, Technische Universität München, Garching bei München, Germany
[2] Dipartimento di Scienze e Tecnologie Aerospaziali, Politecnico di Milano, Milano, Italy

E-mail: `carlo.bottasso@tum.de`

Abstract. Wake steering by active yawing of upstream wind turbines is a promising wind plant control technique. To enable the development of model-based wind plant control methods, there is a need for models that can marry the contrasting requirements of good fidelity and low computational cost. This paper presents a reduced-order model (ROM) obtained by directly compressing high-fidelity computational fluid dynamics (CFD) simulation data using the proper orthogonal decomposition (POD) method. At first, simulations of wake-interacting wind turbines are obtained for time-varying yaw settings using the lifting-line large-eddy simulation (LES) code `SOWFA`. Next, a ROM is synthesized from the CFD transient simulations, obtaining a discrete-time state-space model that captures the dominant dynamics of the underlying high-fidelity model with only a reduced number of states. The ROM is optionally augmented with a Kalman filter, which feeds back turbine power measurements from the plant to the model, enhancing its accuracy. Results obtained in realistic turbulent conditions show a good agreement between high-fidelity CFD solutions and the proposed POD-based ROM in terms of wake behavior and power output of waked turbines. Additionally, the ROM presents acceptable results when compared to wind tunnel experiments, including the capability of the model to partially correct for an intentionally built-in model mismatch.

1. Introduction

Wind turbines are typically installed in clusters, in order to lower construction, maintenance and commissioning costs. However, turbines within a farm are often in close proximity of each other, which has the effect of creating aerodynamic interactions between downstream turbines and the wakes shed by upstream machines. In fact, wakes, which are characterized by a lower wind speed and higher turbulence intensity than the free stream, have a negative impact on the performance of wake-impinged downwind turbines, in turn increasing their loading and reducing their power output. Wind farm control is a newly emerging technology that tries to mitigate these effects.

The central idea of wind farm control is to move away from the current individual optimization of the set point of each single machine, and operate instead the turbines within the plant in a collective (cooperative) manner. This means that machines may be operated at set points that are sub-optimal at the single turbine level, if this creates a benefit at the collective wind plant level. Wake steering, or wake redirection, is a promising technique to implement wind farm control. The idea is in this case to alter the wake path with the goal of reducing the

shading of downstream turbines. Among various possible ways of affecting wake behavior, yaw misalignment —where the rotor is intentionally misaligned with respect to the incoming wind— is the method that is currently more actively being investigated. For example, Refs. [1–3] study wake steering with the help of computational fluid dynamics (CFD) simulations, while Refs. [4,5] use scaled wind turbine models in a boundary layer wind tunnel.

The design of control strategies for wake steering can greatly benefit from models that can faithfully capture all relevant physical processes playing a role in wind turbine wake interactions. This, however, poses significant challenges. In fact, existing engineering models —although typically very fast and using only a limited number of degrees of freedom— might not always be as accurate as desired. In addition, they depend on parameters that need to be calibrated. Although the existence of model parameters offers the possibility of model tuning and adaption, it is also clear that mistuning may hamper the accuracy of the model. On the other hand, CFD-based models are based on first principles. This means that they should have better accuracy and resolution than engineering models, while at the same time they will also have no (or very few) tunable parameters. Unfortunately, they will also come at a very high computational cost. Because of this, their use in the context of control synthesis is extremely challenging, or can actually typically be altogether ruled out [6].

In order to marry the contrasting requirements of high-fidelity and low computational cost, this paper proposes an approach that is based on the idea of compressing high-fidelity CFD data into a reduced-order model (ROM). This is obtained through a data-driven model-identification procedure, based on the proper orthogonal decomposition (POD). The resulting ROMs capture the dominant dynamics of wind turbine wakes and their interactions, while showing at the same time a high degree of data compression. This way, the computationally intensive part of the process is performed offline and, once a ROM has been identified, one is left with a small size state-space model that is ideally suited for the design of model-based control laws.

The paper is organized according to the following structure. Section 2 discusses the characteristics of the simulation environment and considered wind farm control setup. Then, Sect. 3 formulates the methods used for ROM generation. Next, Sect. 4 reports and discusses results, comparing ROM-generated predictions with high-fidelity CFD simulations and wind tunnel experiments. Lastly, conclusions and an outlook towards further developments end the paper in Sect. 5.

2. Simulation environment

2.1. CFD model

First, high-fidelity CFD simulations are performed in order to generate detailed flow data, which is then used to obtain a compressed model (described in Sect. 3). Simulations are run here using a simulation tool based on `SOWFA` (Simulator fOr Wind Farm Applications) [7], which is a lifting-line-based large-eddy simulation (LES) tool developed at the National Renewable Energy Laboratory (NREL), using `OpenFOAM` and coupled with NREL's `FAST` wind turbine structural-dynamics model [8]. The implementation used here features an immersed boundary formulation [9] to model the effects of nacelle and tower, which may have a significant influence on wake development and behavior. Typical simulations last for several days, and were run on the 'SuperMUC' cluster of the Leibniz Supercomputing Centre (LRZ, Germany).

2.2. Simulation setup

The simulations considered here reproduce experiments conducted in the boundary layer wind tunnel of the Politecnico di Milano in Italy, using the G1 (<u>G</u>eneric <u>1</u> m diameter rotor) scaled wind turbine models [5, 10]. The LES CFD environment was validated with respect to experimental data in previous studies [11]. Table 1 reports the main characteristics of the G1 scaled wind turbine models.

Table 1: Main characteristics of the G1 scaled wind turbine model [10].

Rotor diameter (D)	$1.1\,\text{m}$
Hub height	$0.825\,\text{m}$
Rated rotor speed	$850\,\text{rpm}$
Control	Variable speed, pitch, and yaw

The simulation setup considers a two-turbine cluster, where the machines are longitudinally spaced at a distance of 4D and aligned with the prevailing wind flow direction. The free stream flow has an average speed of $5.7\,\text{m/s}$ with a turbulence intensity (TI) of about $6\,\%$ at hub height. Simulations were run with a time step of $0.0004\,\text{s}$ and data was collected in snapshots sampled every $0.01\,\text{s}$ (snapshot frequency of $100\,\text{Hz}$). The stored data includes the power output of both wind turbines, the prescribed upwind turbine yaw control input, and the three velocity components recorded at all grid points on two planes: the first one is a horizontal plane at hub height (termed XY), while the second is a vertical plane going through the center of the two turbine towers (termed XZ). Clearly, although data was collected only at these two planes, simulations consider the full 3D computational domain. A finer mesh was used closer to the turbines and in their wakes, while a coarser one was used elsewhere to reduce computational cost. A description of the grid characteristics on the two planes is provided in Table 2.

Table 2: Grid resolution on the two planes used for data collection.

Plane	Dimensions	Fixed coord.	Resolution	Total points
XY	$\Delta x = 6.2D,\ \Delta y = 1.8D$	$z = 0.825\,\text{m}$	$\delta x = \delta y \approx 0.015D$	$\approx 53{,}000$
XZ	$\Delta x = 6.2D,\ \Delta z = 3.5D$	$y = 3.500\,\text{m}$	$\delta x = \delta z \approx 0.016D$	$\approx 80{,}000$

Data at the generic ith snapshot is collected into column vectors: the three velocity components at each grid point on the two planes (for a total of $N_x \approx 400{,}000$ values) are stored in the state vector $\boldsymbol{x}_i$, the $N_y = 2$ wind turbine powers in the output vector $\boldsymbol{y}_i$, while the $N_u = 1$ upwind turbine yaw angle in the input $\boldsymbol{u}_i$. Next, the various vectors are grouped into snapshot matrices, which are defined as:

$$\mathcal{X} = \begin{bmatrix} \boldsymbol{x}_1 & \boldsymbol{x}_2 & \dots & \boldsymbol{x}_{n_s-1} \end{bmatrix} \in \mathbb{R}^{N_x \times (n_s-1)}, \tag{1a}$$

$$\mathcal{X}' = \begin{bmatrix} \boldsymbol{x}_2 & \boldsymbol{x}_3 & \dots & \boldsymbol{x}_{n_s} \end{bmatrix} \in \mathbb{R}^{N_x \times (n_s-1)}, \tag{1b}$$

$$\mathcal{U} = \begin{bmatrix} \boldsymbol{u}_1 & \boldsymbol{u}_2 & \dots & \boldsymbol{u}_{n_s-1} \end{bmatrix} \in \mathbb{R}^{N_u \times (n_s-1)}, \tag{1c}$$

$$\mathcal{Y} = \begin{bmatrix} \boldsymbol{y}_1 & \boldsymbol{y}_2 & \dots & \boldsymbol{y}_{n_s-1} \end{bmatrix} \in \mathbb{R}^{N_y \times (n_s-1)}, \tag{1d}$$

where n_s is the number of snapshots.

3. Methods
3.1. Model identification signal
In the present approach, ROMs are obtained by a data-driven model-identification procedure. Clearly, any ROM can only include information that is present in the data used for identifying it. Therefore, it is important to excite the system in a proper way during the data generation phase. The excitation signal, which is in this case the yaw input of the upstream turbine, should consider a number of requirements [12,13]: its spectrum should be such that the system response frequencies of interest are properly excited, it should account for limitations in the range of yaw angles and in the yaw rates, and it should be generated with an acceptable length based on

a tradeoff between accuracy and computational time. To account for these characteristics, an APRBS (Amplitude-modulated Pseudo-Random Binary Sequence) signal [12,13] was chosen to excite the system. Such a signal is based on the PRBS signal, a deterministic approximation of white noise in discrete time, which in turn results in a broad-band excitation of the system. Following the recommendations in Refs. [12–14], different values in the range of interest (yaw angles between $\pm 30°$) are assigned to different segments of the signal. This allows for the system to be excited in a wider range of values. Lastly, an APRBS-like yaw input signal is generated by inserting ramps to realistically connect the different steps of the APRBS. A ramp slope (yaw rate) of $30\,°\mathrm{s}^{-1}$ was chosen in agreement with the wind tunnel scaled model characteristics.

3.2. POD-based ROM

From the different ROM formulations proposed in the literature, the approach chosen for the present study is an I/O, data-driven, equation-free, POD-based approach, inspired by the formulation reported in Refs. [15–17]. This modeling procedure is intended to fit and compress the collected data into a standard state-space representation, in order to obtain models of a low computational cost, but also of sufficient quality. A considerable data reduction is obtained by extracting the most dominant features of the simulated system.

The reduced-order system is modeled as an explicit discrete-time time-invariant linear system in state-space form, which writes

$$\begin{cases} \tilde{\boldsymbol{x}}_{k+1} & = \tilde{\boldsymbol{A}}\tilde{\boldsymbol{x}}_k + \tilde{\boldsymbol{B}}\boldsymbol{u}_k, \\ \boldsymbol{y}_k & = \tilde{\boldsymbol{C}}\tilde{\boldsymbol{x}}_k + \tilde{\boldsymbol{D}}\boldsymbol{u}_k, \end{cases} \tag{2}$$

where k is the generic time instant, $\tilde{\boldsymbol{x}}_k \in \mathbb{R}^r$ is the reduced-order state vector, $\boldsymbol{u}_k \in \mathbb{R}^{n_u}$ is the input vector (i.e. the yaw angle of the upstream wind turbine; see Eq. (3)), and $\boldsymbol{y}_k \in \mathbb{R}^{n_y}$ is the output vector (i.e. the power outputs of the two turbines). Scalar r represents the order —or number of states— of the ROM. Matrices $\tilde{\boldsymbol{A}}$, $\tilde{\boldsymbol{B}}$, $\tilde{\boldsymbol{C}}$ and $\tilde{\boldsymbol{D}}$ have the appropriate dimensions.

In order to address non-linearities in the system and to improve the accuracy of the model, the input vector $\boldsymbol{u}_k$ was enriched so as to better capture the effects of yaw angle variations on the flow states $\tilde{\boldsymbol{x}}_k$ and power output $\boldsymbol{y}_k$. To this end, the input vector is defined as

$$\boldsymbol{u}_k = \boldsymbol{f}(\gamma_k) = (\gamma_k, \gamma_k^2, \gamma_k^3, \gamma_k^4, \cos^p(\gamma_k) - 1)^T, \tag{3}$$

where γ_k is the prescribed yaw angle. The non-linear relationship between yaw input and the variations of flow states and power outputs is modeled by the combination of a fourth order polynomial and a $\cos^p$ term. The latter is included considering the experimentally-derived relationship between yaw angle and power output [18], using the value $p = 1.787$. Regarding the system non-linearities that the polynomial fit partially handles, it should be noted that power is largely independent on the sign of the yaw angle misalignment. For this reason, even functions are required for properly modeling the relationship between yaw misalignment and power. Odd terms are also needed to match the behavior of the flow velocity components, and to handle any lack of symmetry in power output for positive and negative yaw angles.

The reduced-order state vector is obtained by projecting the full-order state vector $\boldsymbol{x}_k \in \mathbb{R}^{n_x}$ onto a lower-dimensional subspace of dimension r (typically, $n_x \gg r$). The relation between the full-order state vector and the reduced-order one is defined as:

$$\tilde{\boldsymbol{x}}_k = \boldsymbol{P}\boldsymbol{x}_k, \tag{4}$$

where $\boldsymbol{P} \in \mathbb{R}^{r \times n_x}$ is the projection subspace matrix. A suitable choice for the projection subspace matrix [15–17] is obtained by performing a singular value decomposition (SVD) of the snapshot matrix $\mathcal{X}$ of Eq. (1), which writes

$$\mathcal{X} = \boldsymbol{U}\boldsymbol{\Sigma}\boldsymbol{V}^T, \tag{5}$$

where $\boldsymbol{U} \in \mathbb{R}^{n_x \times (n_s-1)}$ contains the left-singular vectors, $\boldsymbol{\Sigma} \in \mathbb{R}^{(n_s-1) \times (n_s-1)}$ the singular values and $\boldsymbol{V} \in \mathbb{R}^{(n_s-1) \times (n_s-1)}$ the right-singular vectors of $\mathcal{X}$. The left-singular vectors are, indeed, the so-called POD modes (POMs) of the system [19,20]. Using such modes for the generation of the subspace projection provides for major benefits, since POMs represent a series of intrinsic patterns of the flow (specifically, spatial and non-temporal ones). The temporal description, i.e. the evolution of the POMs over time, can be extracted from the right-singular vectors. Finally, the energy, or the weight, of each one of the POMs is given by the corresponding singular value.

The advantage of this decomposition is that, by only retaining a subset r of the POD modes, a high degree of compression of the original data can be obtained while still preserving a satisfactory modeling accuracy. In fact, the approximation of $\mathcal{X}$ can be written as

$$\mathcal{X} = \boldsymbol{U}\boldsymbol{\Sigma}\boldsymbol{V}^T = \begin{bmatrix} \boldsymbol{U}_r & \boldsymbol{U}_{n_s-1-r} \end{bmatrix} \begin{bmatrix} \boldsymbol{\Sigma}_r & \boldsymbol{0} \\ \boldsymbol{0} & \boldsymbol{\Sigma}_{n_s-1-r} \end{bmatrix} \begin{bmatrix} \boldsymbol{V}_r & \boldsymbol{V}_{n_s-1-r} \end{bmatrix}^T \simeq \boldsymbol{U}_r \boldsymbol{\Sigma}_r \boldsymbol{V}_r^T, \tag{6}$$

where $(\cdot)_r$ and $(\cdot)_{n_s-1-r}$ indicate a partitioning of the SVD matrices $\boldsymbol{U}, \boldsymbol{\Sigma}$ and $\boldsymbol{V}^T$. As previously stated, the projection subspace matrix that relates full- and reduced-order states is represented by the POD modes of the original system. In particular, a selection is used of the first r POD modes, i.e. the most energetic ones (characterized by higher singular values), which are also the ones typically associated with lower frequencies (and that are hence better resolved). This results in the following projection subspace matrix:

$$\boldsymbol{P} := \boldsymbol{U}_r^T. \tag{7}$$

Since $\boldsymbol{U}_r$ is a real orthogonal matrix formed by orthogonal unit vectors arranged in columns, the following relation holds

$$\boldsymbol{P}\boldsymbol{P}^T = \boldsymbol{I}_r, \tag{8}$$

where $\boldsymbol{I}_r$ is the $r \times r$ identity matrix.

Finally, consider the system of Eq. (2) expressed in compact form, i.e.

$$\begin{bmatrix} \tilde{\mathcal{X}}' \\ \mathcal{Y} \end{bmatrix} = \begin{bmatrix} \tilde{\boldsymbol{A}} & \tilde{\boldsymbol{B}} \\ \tilde{\boldsymbol{C}} & \tilde{\boldsymbol{D}} \end{bmatrix} \begin{bmatrix} \tilde{\mathcal{X}} \\ \mathcal{U} \end{bmatrix}, \tag{9}$$

where $\tilde{\mathcal{X}}'$ and $\tilde{\mathcal{X}}$ are the projections of $\mathcal{X}'$ and $\mathcal{X}$, respectively, onto the lower-dimensional subspace via matrix $\boldsymbol{P}$. Substituting the expressions of Eq. (4) and Eq. (7) into Eq. (9), the matrices defining the reduced-order state-space system can be readily obtained as:

$$\begin{bmatrix} \tilde{\boldsymbol{A}} & \tilde{\boldsymbol{B}} \\ \tilde{\boldsymbol{C}} & \tilde{\boldsymbol{D}} \end{bmatrix} = \begin{bmatrix} \boldsymbol{U}_r^T \mathcal{X}' \\ \mathcal{Y} \end{bmatrix} \begin{bmatrix} \boldsymbol{U}_r^T \mathcal{X} \\ \mathcal{U} \end{bmatrix}^\dagger. \tag{10}$$

4. Results
The model-compression procedure explained in the previous section was applied to raw CFD data in order to obtain the desired ROM. To this end, an APRBS signal was designed to excite the system by changing the upwind turbine yaw angle. The length of the training simulation was set to $60\,\mathrm{s}$, which was considered long enough to appropriately excite the system within the range of $\pm 30°$, while limiting the computational costs. Then, the procedure explained in Sect. 3 was applied, resulting in a ROM with 22 POD modes. The order of the model was chosen as a best compromise between model size and error between high-fidelity and reduced-order-reconstructed flow and power outputs.

Subsequently, a second CFD simulation was performed with a different input signal to validate the prediction capabilities of the previously obtained ROM. The ROM was verified for this validation test case in two different variants: in conjunction with a Kalman filter (KF) state observer [21], which uses the power measured at the two machines to estimate and update the model state vector, and in open loop. The process noise covariance matrix of the KF (Q_k) was tuned by differently weighting each element of the reduced-order state, i.e. each POD mode. Specifically, modes with higher energies and better resolution (low frequency spectra) were assigned smaller covariances. The measurement noise covariance matrix R_k was set to a low value, since power measurements can be assumed to be highly accurate.

A few of the POD modes of the system are displayed in Fig. 1. Each POM includes the three velocity components for the two planes of data collection; however, only the horizontal plane and the streamwise velocity component are plotted in Fig. 1. The low-index POD modes exhibit patterns that are consistent with the expected behavior resulting from an excitation by yawing of the upwind turbine, and indicate large spatial variations of the flow. High-index POMs (e.g. number 200 in Fig. 1) preserve, on the other hand, the high-fluctuating spatial behavior of the underlying high-fidelity data, and are therefore associated with lower energies. As explained in Sect. 3, POMs are also associated to a specific frequency content, stored in the right-singular vectors of the SVD. Commonly, POMs with low indices present also low-frequency spectra, and vice versa. Indeed, a frequency analysis (discrete Fourier transform, DFT) was performed for the POMs retained in the ROM. Their frequency spectrum was found to be below 15 Hz. Given that the Nyquist frequency associated with the sampling frequency is 50 Hz, this result ensures that the sampling is large enough to capture the mode dynamics.

A comparison of the power outputs of the validation case CFD simulation and ROM reconstruction is shown in Fig. 2. The power variations of both turbines predicted by the model is given directly in the model output vector, as stated in Eq. (2). The use of the Kalman filter —which feeds power measurements from the plant back to the ROM— improves the quality of predictions. Indeed, the time-averaged percentage error between CFD and ROM-predicted power outputs reduced from 3.83%, 6.68% and 3.64% for the case without KF, to 1.81%, 3.98% and 1.89% for the case with KF, where the three values refer to the upstream turbine (WT1), the downstream one (WT2) and the whole cluster, respectively. In open-loop, the model does not receive any information from the plant regarding power changes due to flow fluctuations. This appears clearly in the figure where, for constant yaw angles, the model cannot accurately predict the fluctuating behavior of power other than the intrinsic dynamics contained in the ROM.

The reconstructed full-order flow produced by the ROM can be approximated combining Eqs. (4) and (7). A comparison between CFD high-fidelity data and ROM-based reconstructed flow is shown in Figs. 3 and 4 for a given instant in time. ROM predictions, with and without state observer, match the average wake shape and position. On the other hand, smaller scale fluctuations and wake meandering are not captured. Notice further that the Kalman filter is capable of enhancing the behavior of the model in terms of power predictions, without visually substantially affecting the macroscopic flow behavior in the wake.

Finally, the behavior of the model was also tested with data from a wind tunnel experiment [5], under very similar conditions in terms of yaw dynamic changes, inflow and turbulent intensity of the numerical test conducted so far. However, crucially, in the wind tunnel experiments the two turbines were spaced 5D, while the simulations used to generate the ROM used a spacing of only 4D. In other words, the ROM was created on purpose with a significant built-in model mismatch. The ROM predictions are compared with the experimental data in terms of turbine power outputs in Fig. 5. It is observed, indeed, that the predicted power for the downwind turbine is always smaller than the actual one. This is expected, since in the experiment the wake recovered further before impinging onto the downstream wind turbine, due to the larger
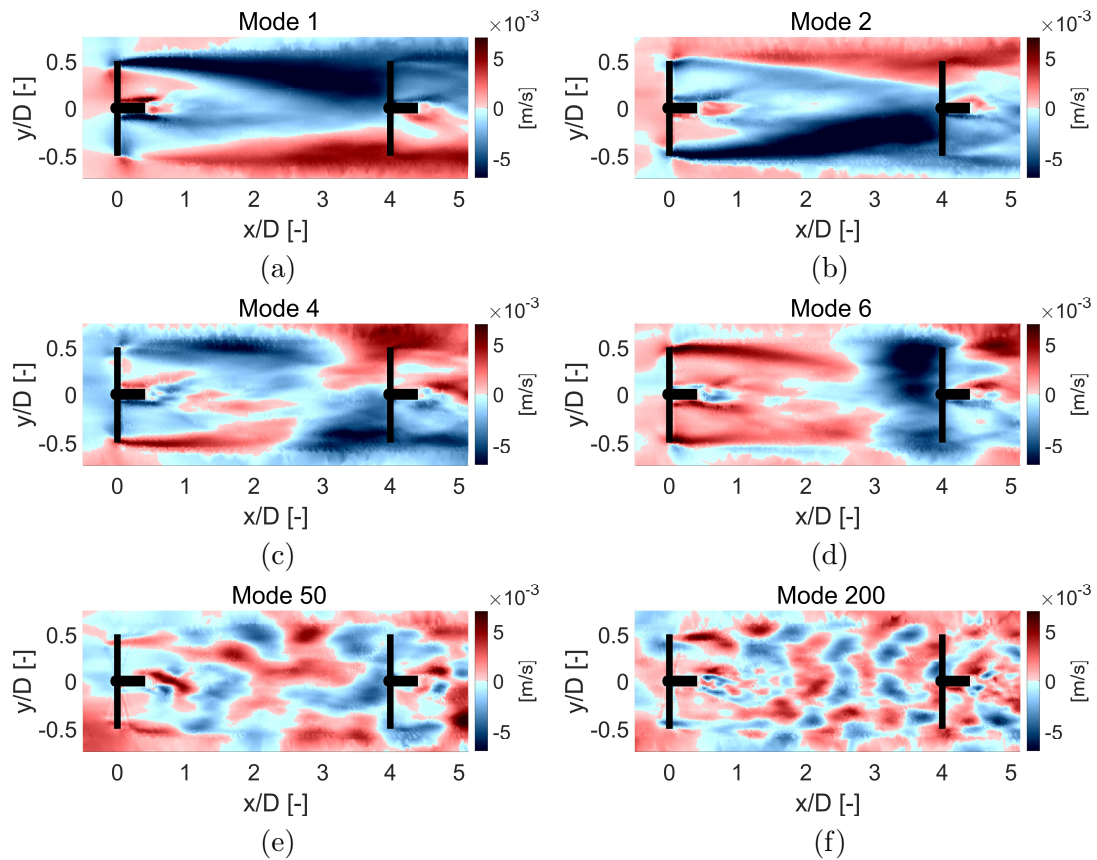
Figure 1: Selection of POD modes of the simulated system (only the mode streamwise velocity components in the XY plane are shown).

distance between the two machines. The KF is able to partially correct for this model defect. For the upwind turbine, the prediction fluctuates but does not present a systematic bias, as there is not a model mismatch in this case. Even considering the error due to the different wind farm layout, the ROM seems to be capable of predicting the power outputs with acceptable accuracy.

5. Conclusions and outlook

In this paper, a compression technique based on the POD is applied to obtain ROMs with very low computational cost and good accuracy, suitable for model-based wind farm control. The present study has focused on a two-turbine cluster, where yaw misalignment of the front machine is used for wake steering. To further improve the quality of predictions, the resulting ROM has been optionally equipped with a KF, which feeds power measurements from the plant back onto the model. Results indicate that the proposed method is able to represent well, when compared to high-fidelity CFD-simulated data, the wake characteristics of both turbines and their respective power outputs. Regarding flow predictions, a proper deflection and development of the wake is observed. With respect to power outputs, the predictions are also accurate and correlate well with changes in the upwind turbine yaw angle. When compared to wind tunnel experiments, acceptable results are also obtained, including the capability of the model to partially correct for an intentionally built-in model mismatch.

The present work will be expanded in multiple directions. Regarding model updating, it
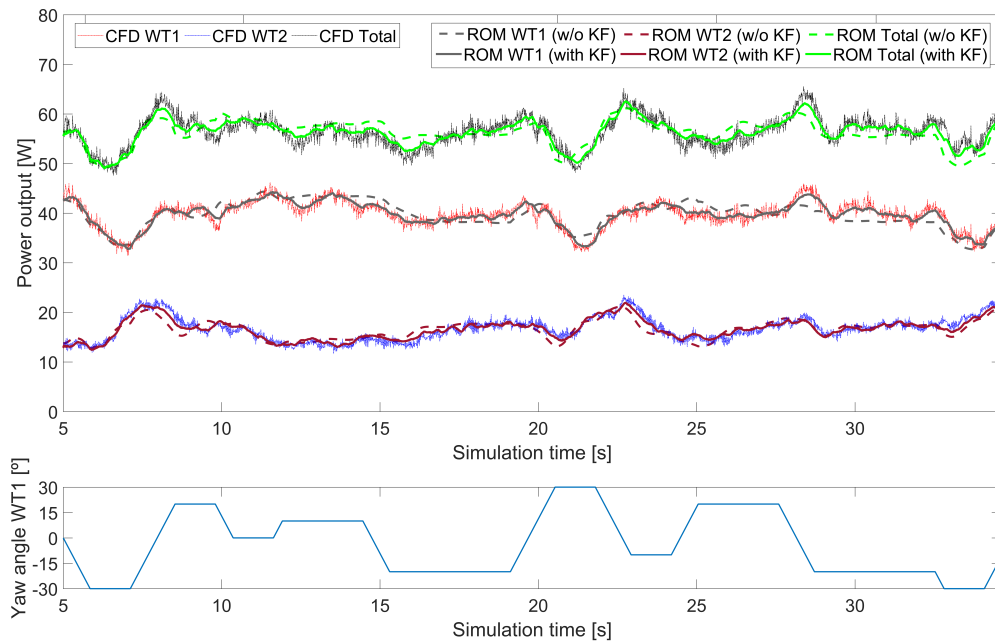
Figure 2: Comparison between CFD data and ROM-predicted power outputs (top); yaw angle time history for the upstream wind turbine (bottom).
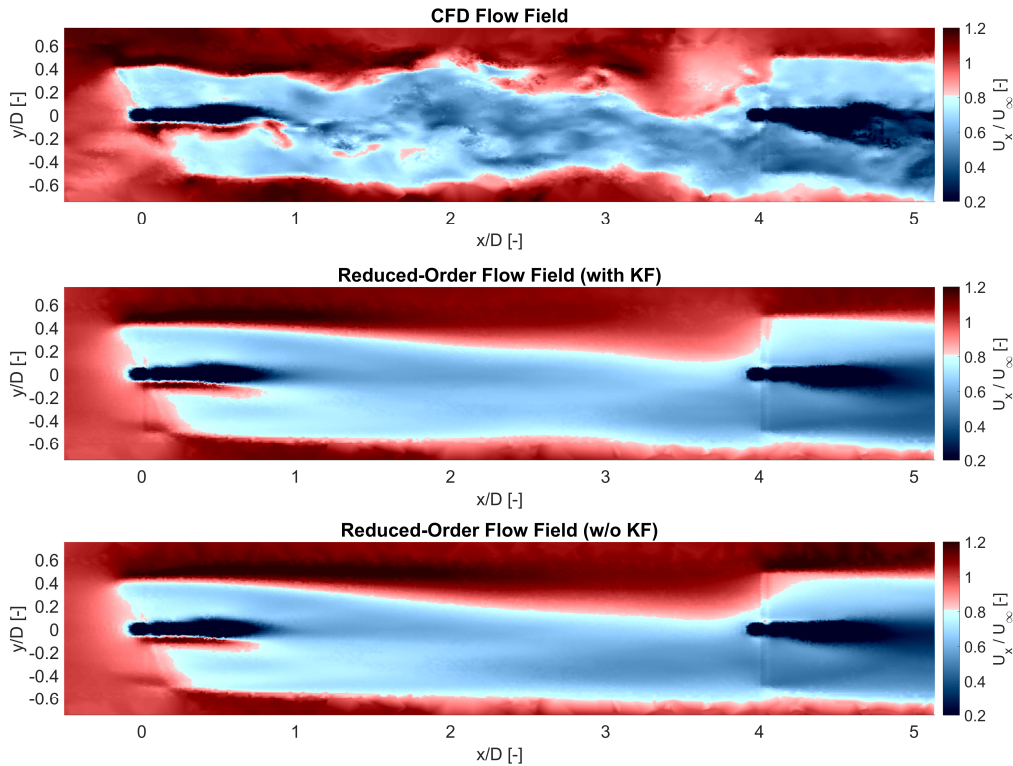

Figure 3: Comparison of the streamwise velocity component on the horizontal plane between the CFD flow (top), ROM-predicted flow with KF state observer (middle), and ROM-predicted flow without state observer (bottom) at one instant in time ($\gamma = 23°$).
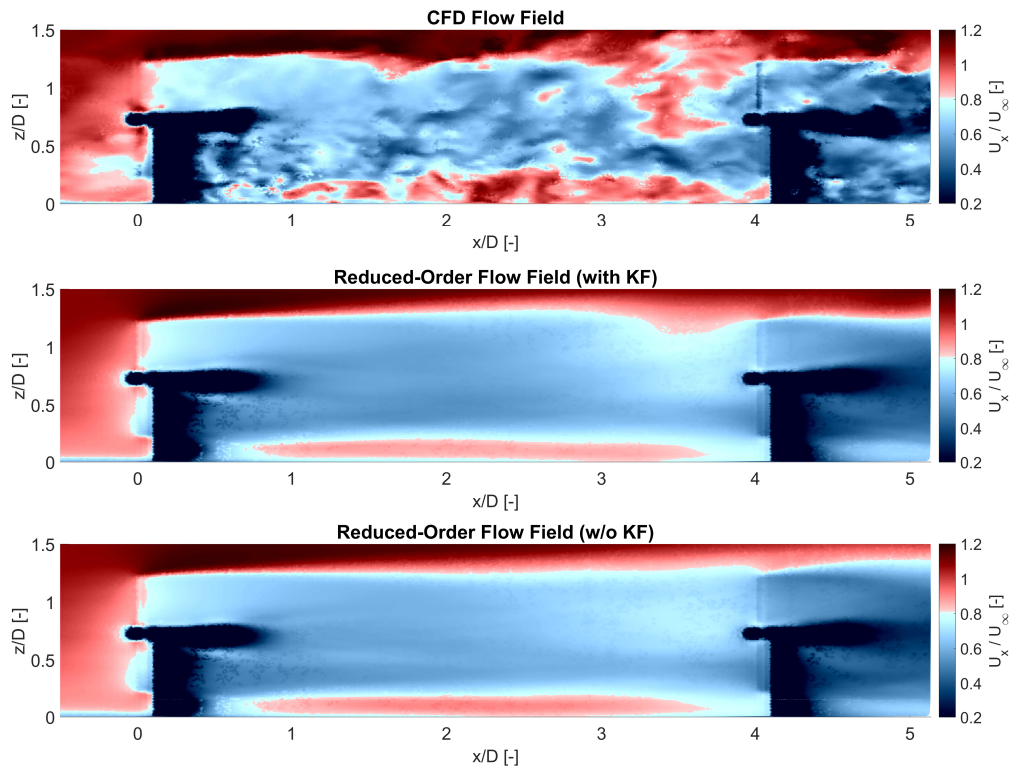
Figure 4: Comparison of the streamwise velocity component on the vertical plane between the CFD flow (top), ROM-predicted flow with KF state observer (middle), and ROM-predicted flow without state observer (bottom) at one instant in time ($\gamma = 23°$).
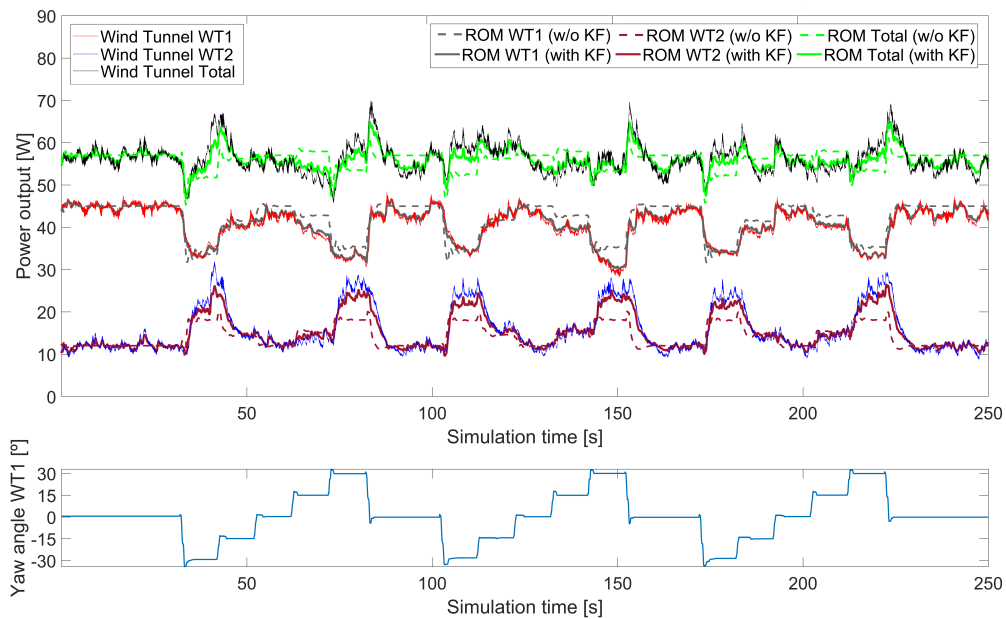

Figure 5: Comparison between wind tunnel and ROM-predicted power outputs considering a model mismatch (top); yaw angle time history for the upstream wind turbine (bottom).

should be mentioned that, in addition to power, other plant measurements can be used to improve the predictive capabilities of the method. For example, Ref. [22] uses local estimates of the wind speed on the rotor disk, obtained by using blade load measurements. Additional work will try to improve the generality of the approach. In fact, since the method is based on system identification, ROMs are derived for a particular configuration and operating condition (wind farm layout, wind speed, TI, etc.). If other conditions are desired, additional high-fidelity CFD simulations are required (cf. [23]). While this problem cannot be completely bypassed, there are techniques that we are currently exploring to reduce the complexity of the approach and its associated computational effort.

Acknowledgments

References

[1] Fleming P A, Gebraad P M O, Lee S, van Wingerden J-W, Johnson K, Churchfield M, Michalakes J, Spalart P and Moriarty P 2014 *Renew. Energ.* **70** 211-8
[2] Gebraad P M O, Teeuwisse F W, van Wingerden J-W, Fleming P A, Ruben S D, Marden J R and Pao L Y 2014 *American Control Conference (ACC), 2014* 3128–34
[3] Gebraad P M O, Teeuwisse F W, van Wingerden J-W, Fleming P A, Ruben S D, Marden J R and Pao L Y 2016 *Wind Energ.* **19** 95–114
[4] Wang J, Bottasso C L and Campagnolo F 2016 *J. Phys.: Conf. Series* **753** 32064
[5] Campagnolo F, Petrović, Schreiber J, Nanos E M, Croce A and Bottasso C L 2016 *J. Phys.: Conf. Series* **753** 32006
[6] Munters W and Meyers J 2017 *Phil. Trans. R. Soc. A.* **375** 20160100
[7] Churchfield M and Lee S 2012 NWTC design codes-SOWFA URL: `https://nwtc.nrel.gov/SOWFA`
[8] Jonkman J M and Buhl Jr. M L 2005 FAST User's Guide-Updated August 2005 *National Renewable Energy Laboratory (NREL), Golden, CO (United States)*
[9] Mittal R and Iaccarino G 2005 *Annu. Rev. Fluid Mech.* **37** 239–61
[10] Bottasso C L, Campagnolo F and Petrović V 2014 *J. Wind Eng. Ind. Aerod.* **127** 11–28
[11] Wang J, Foley S, Nanos E M, Yu T, Campagnolo F, Bottasso C L, Zanotti A and Croce A 2017 *J. Phys.: Conf. Series* **854** 012048
[12] Isermann R and Münchhof M 2010 *Identification of Dynamic Systems: an Introduction with Applications* (Springer Science & Business Media)
[13] Nelles O 2013 *Nonlinear System Identification: from Classical Approaches to Neural Networks and Fuzzy Models* (Springer Science & Business Media)
[14] Deflorian M and Zaglauer S 2011 *IFAC Proc. Vol.* **44** 13179–84
[15] Annoni J, Gebraad P M O and Seiler P 2016 *American Control Conference* 506–12
[16] Proctor J L, Brunton S L and Kutz J N 2016 *SIAM J. Appl. Dyn. Syst.* **15** 142–61
[17] Annoni J, Nichols J and Seiler P 2016 *34th Wind Energy Symposium* 2201
[18] Schreiber J, Nanos E M, Campagnolo F and Bottasso C L 2017 *J. Phys.: Conf. Series* **854** 012041
[19] Holmes P 2012 *Turbulence, Coherent Structures, Dynamical Systems and Symmetry* (Cambridge University Press)
[20] Kerschen G and Golinval J-C 2002 *J Sound Vib.* **249** 849–65
[21] Kalman R E 1960 *J. Basic Eng.* **82** 35–45
[22] Bottasso C L, Cacciola S and Schreiber J 2018 *Renew. Energ.* **116** 155–68
[23] Annoni J and Seiler P 2017 *Int. J. Robust Nonlinear Control* **4** 582–97